

OPEN

# Impaired functional capacity of polarised neonatal macrophages

Stephan Dreschers<sup>1</sup>, Kim Ohl<sup>2</sup>, Nora Schulte<sup>2</sup>, Klaus Tenbrock<sup>2</sup> & Thorsten W. Orlikowsky<sup>1\*</sup>

Neonatal sepsis is accompanied by impaired apoptotic depletion of monocytes and macrophages (M $\Phi$ ), aberrant cytokine production, impaired cell metabolism, and sustained inflammation. Macrophage-colony stimulating factor (M-CSF) triggers the differentiation from monocytes into M $\Phi$  (M $\Phi$ -0). Interleukin-10 (IL10) and Interferon-gamma (IFN $\gamma$ ) further differentiate M $\Phi$  subpopulations, the anti-inflammatory M $\Phi$ -IL10 and the pro-inflammatory M $\Phi$ -IFN $\gamma$  subtype. We previously have shown significant differences between adult (PBM $\Phi$ ) and cord blood (CBM $\Phi$ ) in the metabolism of all subtypes. To test the hypothesis whether the competence to differentiate monocytes into M $\Phi$ -0 and to polarise into M $\Phi$ -IFN $\gamma$  and M $\Phi$ -IL10 was diminished in CBM $\Phi$  as compared to PBM $\Phi$ , we polarised monocytes by cultivation with M-CSF for 72 h, followed by stimulation with IFN $\gamma$  or IL10, for 48 h. After flow cytometry based immunotyping, we tested four functions: Phagocytosis of GFP-*E. coli*, uptake of erythrocytes, T-cell proliferation, induction of regulatory T-cells as well as phosphorylation analysis of AKT and STAT1/STAT3. Phosphorylation of STAT-1 and STAT-3, obligatory to differentiate into M $\Phi$ -IFN $\gamma$ , M $\Phi$ -0 and M $\Phi$ -IL10, was found to be aberrant in CBM $\Phi$ . Whereas infected M $\Phi$ -0 showed identical phagocytic indices and intracellular degradation, TLR4-expression, NF $\kappa$ B up-regulation, IL10-, IL6-, and TNF $\alpha$  production of CBM $\Phi$ -0 were reduced. In addition, the capacity to bind aged erythrocytes and the consecutive IL10 production was lower in CBM $\Phi$ -IL10. Polarised PBM $\Phi$ -IFN $\gamma$  and PBM $\Phi$ -IL10 expressed higher levels of co-stimulatory receptors (CD80, CD86), had a higher capacity to stimulate T-cells and induced higher amounts of regulatory T-cells (all  $p < 0.05$  vs. corresponding CBM $\Phi$ ). Hypoxia-inducible-factor-1 $\alpha$  (HIF-1 $\alpha$ ) was stronger expressed in CBM $\Phi$ -IFN $\gamma$  and upregulated in infected CBM $\Phi$ -0, whereas heme-oxygenase 1 (HO-1) expression was similar to adult PBM $\Phi$ . Neonatal M $\Phi$ -0, M $\Phi$ -IFN $\gamma$  and M $\Phi$ -IL10 polarisation is impaired with respect to phenotype and functions tested which may contribute to sustained inflammation in neonatal sepsis.

Macrophages (M $\Phi$ ) have an extremely broad spectrum of functions in both the induction and resolution of inflammation due to their heterogeneity and plasticity. They are involved in a range of processes, including tissue homeostasis, clearance or pulmonary surfactant as well as inflammation. Deriving from monocytes, they develop into different populations of circulating inflammatory or resident macrophages (M $\Phi$ ) recruited to various tissues. These processes occur in response to inflammation or infection but also in homeostasis in order to replace apoptotic (M $\Phi$ )<sup>1</sup>. The migration of monocytes to the site of infection is crucial<sup>2</sup>. After infiltrating the infected tissue they polarise into functional distinguishable M $\Phi$ . The term “polarisation” instead of differentiation became accepted, since this process depends on the local cytokine milieu and specific microenvironmental cues, and therefore is reversible<sup>3,4</sup>.

By analogy to T helper cell (Th) nomenclature, M $\Phi$  have been classified into two categories: type 1 or classically activated (M1-) and type 2 or alternatively activated M2-M $\Phi$ . *In-vitro*, peripheral monocytes can be polarised by M-CSF, GM-CSF or G-CSF into non-polarised M $\Phi$ <sup>5</sup>. M1 type M $\Phi$  originate from monocytes stimulated with GM-CSF or M-CSF in the presence of IFN- $\gamma$  and/or bacterial products. In contrast, M2 type M $\Phi$  are polarised by M-CSF and IL-4 or IL-13 (M2a), immune complexes together with lipopolysaccharide (LPS) or IL-1 $\beta$  (M2b), and M-CSF and IL10 or glucocorticoids (GC) respectively (M2c), reviewed in<sup>6</sup>.

M1 and M2 type M $\Phi$  can be roughly categorized regarding their function. M1-M $\Phi$  display high microbicidal activity and suppress tumor growth, whereas M2-M $\Phi$  are characterized by an enhanced phagocytic capacity which is shaped to eliminate cellular and apoptotic debris rather than to neutralize pathogens. This, so called, M1/M2 paradigm was refaced, since it became difficult to classify M $\Phi$  subsets comprehensively<sup>7</sup>.

<sup>1</sup>Section of Neonatology, University Children's Hospital, Aachen, 52074, Germany. <sup>2</sup>Department of Pediatrics, RWTH Aachen University, Aachen, Germany. \*email: [torlikowsky@ukaachen.de](mailto:torlikowsky@ukaachen.de)

From the transcriptional level, administration of LPS or IFN $\gamma$  dramatically activates up to 90% of genes giving rise to M1-M $\Phi$ . These M1-M $\Phi$  are polarised from monocytes, which are - under physiological conditions - constantly exposed to M-CSF establishing naïve, “standby” M $\Phi$ . In this manuscript they are termed M $\Phi$ -0.

In M2-M $\Phi$  subsets transcriptome changes are more distinct. Therefore, today's nomenclature is based on more distinct “sensor” and “effector” molecule expressions<sup>8</sup>. According to the expression of receptors, intracellular factors and secreted cytokines, M2-M $\Phi$  subsets are renamed to M $\Phi$ -IL4/M $\Phi$ -IL13 (replacing M2a), M $\Phi$ -IC (replacing M2b) and M $\Phi$ -IL10 (replacing M2c). This nomenclature is used in the present manuscript.

Upon infection, M $\Phi$ -0 are polarised by pathogen-activation-pattern-molecules (PAMPs) to M $\Phi$ -IFN $\gamma$ , exhibiting a “kill/fight” status, which is accompanied with secretion of inflammatory cytokines, reactive-oxygen-status (ROS) and nitric oxide (NO). After neutralization of the pathogens a substantial reprogramming of M $\Phi$ -IFN $\gamma$  starts to skew pro- to anti-inflammatory responses. The M $\Phi$  status is set to “fix/heal”<sup>9</sup>. The M2-M $\Phi$  are also reported to be important for matrix deposition and tissue remodeling<sup>5</sup>.

This functional transition of M $\Phi$  subpopulations is a crucial phase to avoid the individual of being harmed by either incomplete neutralization of pathogens or sustained inflammation. Compared to adults the immune system of newborns is less experienced to execute this transition to resolve inflammation and therefore more vulnerable<sup>10</sup>.

Reports concerning M $\Phi$  polarisation from neonatal monocytes in *ex-vivo* setups are rare. We have previously shown that CBM $\Phi$  exhibit reduced expression of phagocytosis receptors and cytokines in addition to altered energy metabolism. In particular, IFN $\gamma$  as well as IL10 activated CBM $\Phi$  completely fail to increase glycolysis and furthermore show reduced activation of the mTOR pathway, which is important for survival in sepsis<sup>11</sup>. Reduced polarisation capacity is likely to suppress M $\Phi$  functions in neonates, such as activation and expansion of specialized T-cell subpopulations. In line with this observation, they were found to be less efficient in antigen presentation<sup>12</sup>. We thereby observed that scavenger receptors, e.g. CD163, and Fc receptors, critically involved in phagocytosis of bacteria and cellular debris, i.e. elimination of haemoglobin-haptoglobin complexes (Hb:Hp), are overexpressed in M $\Phi$ -IL10 from adults (PBM $\Phi$ -IL10) but not in newborns (CBM $\Phi$ -IL10)<sup>4,11</sup>.

An aberrant polarisation of CBM $\Phi$  can also be caused by immune cell populations specific for the neonatal period of life. CD71<sup>+</sup> erythroid cells as well as myeloid derived suppressor cells (MDSCs) were described to reduce pro-inflammatory processes after bacterial infections<sup>13,14</sup>. The exact role of CD71<sup>+</sup> erythroid cells and MDSCs is still controversial, since the newborn can either benefit or be harmed from effects maintained by these cells.

M $\Phi$  polarisation attracted interest, because the development of therapeutical strategies could benefit from a temporal programming of immune cells. This is especially true for M $\Phi$ -IL10, which can be polarised by administration of GC. Recent publications reported an increase in M2-M $\Phi$  after GC treatment and an improved outcome in acute lung injury<sup>15</sup>. Patients with therapeutically polarised M $\Phi$ -IL10 recovered with a better outcome from asthma<sup>16</sup>. M $\Phi$  are a target in neonatal hypoxic ischemic encephalopathy (HIE) for being programmed to M2- M $\Phi$ <sup>17</sup>.

Here we tested the hypothesis that CBM $\Phi$  exhibit reduced phenotypic and functional characteristics in comparison to PBM $\Phi$ . We have previously shown that CBM $\Phi$  are less responsive to polarise further into CBM $\Phi$ -IL10, thus exhibiting a higher risk to contribute to sustained inflammation.

To this end, we compared the expression of surface markers on M $\Phi$ -0 and M $\Phi$ -IL10, derived from either cord blood or peripheral blood of adult donors. Furthermore, we investigated the expression of the intracellular signal transducers STAT1/STAT3 and PI3K/AKT, which are engaged in infection-induced signaling via TLR4 and contribute to cytokine- as well as CD163 expression. We quantified HIF-1 $\alpha$  and HO-1 levels, which link primary immune responses like pathogen-associated-molecular pattern (PAMP) recognition, cytokine production and metabolism. Finally, we analysed the M $\Phi$ -dependent T cell activation and induction of regulatory T cells.

## Results

**Activated STAT-kinase expression drives polarisation of PBM $\Phi$  but is impaired in CBM $\Phi$  subsets.** We cultivated monocytes (either peripheral blood monocytes (PBMO) or cord blood monocytes (CBMO) under conditions, which differentiate these cells into M $\Phi$ -0 and further lead to their development into either pro-inflammatory M $\Phi$ -IFN $\gamma$  or anti-inflammatory M $\Phi$  subsets such as M $\Phi$ -IL4, M $\Phi$ -IL10 and M $\Phi$ -IL13.

We extended our previous studies by assessing the phosphorylation status of the intracellular signal transducers STAT-1 and STAT-3, which have been shown to be obligatory for proper polarisation to the subtypes of M $\Phi$ -IFN $\gamma$ , M $\Phi$ -0 and M $\Phi$ -IL10<sup>7</sup> (Fig. 1A,B). Under IFN $\gamma$  cultivation, PBM $\Phi$  showed highest STAT1 phosphorylation and lower STAT-1 phosphorylation in M $\Phi$ -0 and M $\Phi$ -IL10, as already described<sup>7</sup>. In contrast, CBM $\Phi$  exhibited an aberrant STAT-1 phosphorylation profile: Whereas the M $\Phi$ -0 type showed a comparable STAT-1 phosphorylation to adult PBM $\Phi$ , CBM $\Phi$ -IFN $\gamma$  and CBM $\Phi$ -IL10 displayed less STAT-1 phosphorylation (Fig. 1A).

STAT3 phosphorylation was significantly stronger in PBM $\Phi$ -0 and in PBM $\Phi$ -IL10 compared to corresponding CBM $\Phi$  subtypes (Fig. 1B). Taken together, PBM $\Phi$  responded to cytokine driven polarisation with higher levels of activated STAT1 in PBM $\Phi$ -IFN $\gamma$  and higher activated STAT3 in PBM $\Phi$ -IL10.

Next, we analysed two nuclear factors, hypoxia-inducible factor-1alpha (HIF-1 $\alpha$ ) and heme-oxygenase-1 (HO-1). HIF-1 $\alpha$  was most highly expressed in PBM $\Phi$ -IFN $\gamma$  (Fig. 1C). PBM $\Phi$ -0 and PBM $\Phi$ -IL10 contained lower intracellular HIF-1 $\alpha$  concentrations. CBM $\Phi$  exhibited a comparable expression profile, however the expression of HIF-1 $\alpha$  in both, CBM $\Phi$ -0 and CBM $\Phi$ -IFN $\gamma$  was two times higher compared to their adult counterparts. The anti-inflammatory HO-1 was found expressed most strongly in PBM $\Phi$ -IL10 and CBM $\Phi$ -0 (Fig. 1D). In summary, the results suggest that M $\Phi$  from adults polarised as previously shown and expected, whereas CBM $\Phi$  exhibited an aberrant polarisation profile.

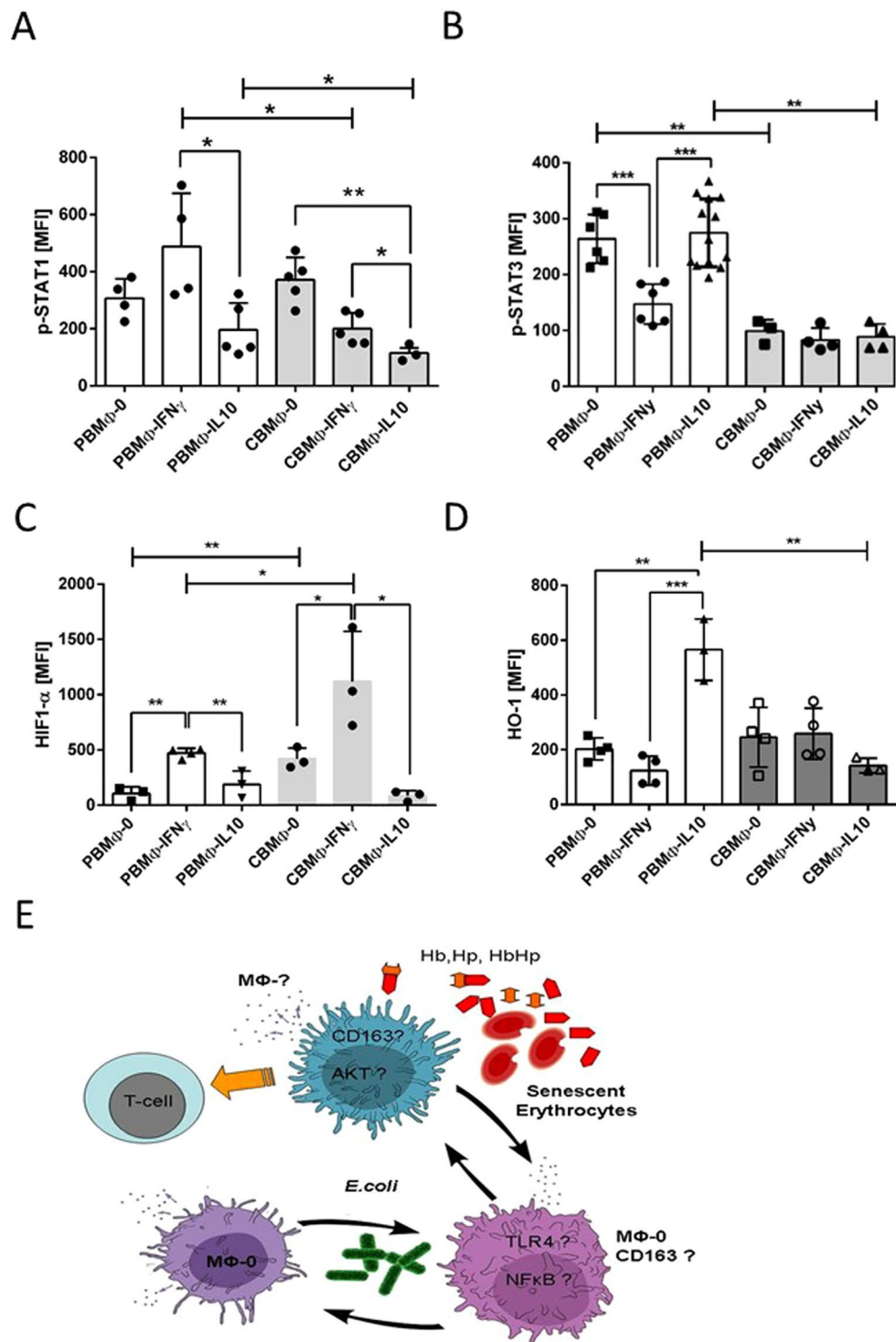


**Figure 1.** STAT-1/STAT-3 phosphorylation status in M $\Phi$  subsets. M $\Phi$  subsets were further analysed for STAT-1 (A) and STAT-3 phosphorylation (B), Furthermore, the intracellular levels of HIF-1 $\alpha$  (C) and HO-1 were determined (D, \* $p < 0.05$ , \*\* $p < 0.01$ , \*\*\* $p < 0.005$ ; bars, student's t-test, blunt ended bars, two-way-ANOVA). Sketch (E) summarizes the investigations regarding to M $\Phi$  and T cells and the indicated stimuli. Cytokine release of M $\Phi$  is represented by dots and small arrows. Question marks represent cellular factors whose expression will be examined in Figs. 2–5.

In order to analyse functional consequences, we challenged CBM $\Phi$ -0 and CBM $\Phi$ -IL10 with *Escherichia coli* (*E. coli*), or Hb:Hp complexes from senescent erythrocytes (EL). In particular, we focused on keyplayers of TLR4/NF $\kappa$ B and CD163/AKT/IL10 signaling pathway (see sketch Fig. 1E).

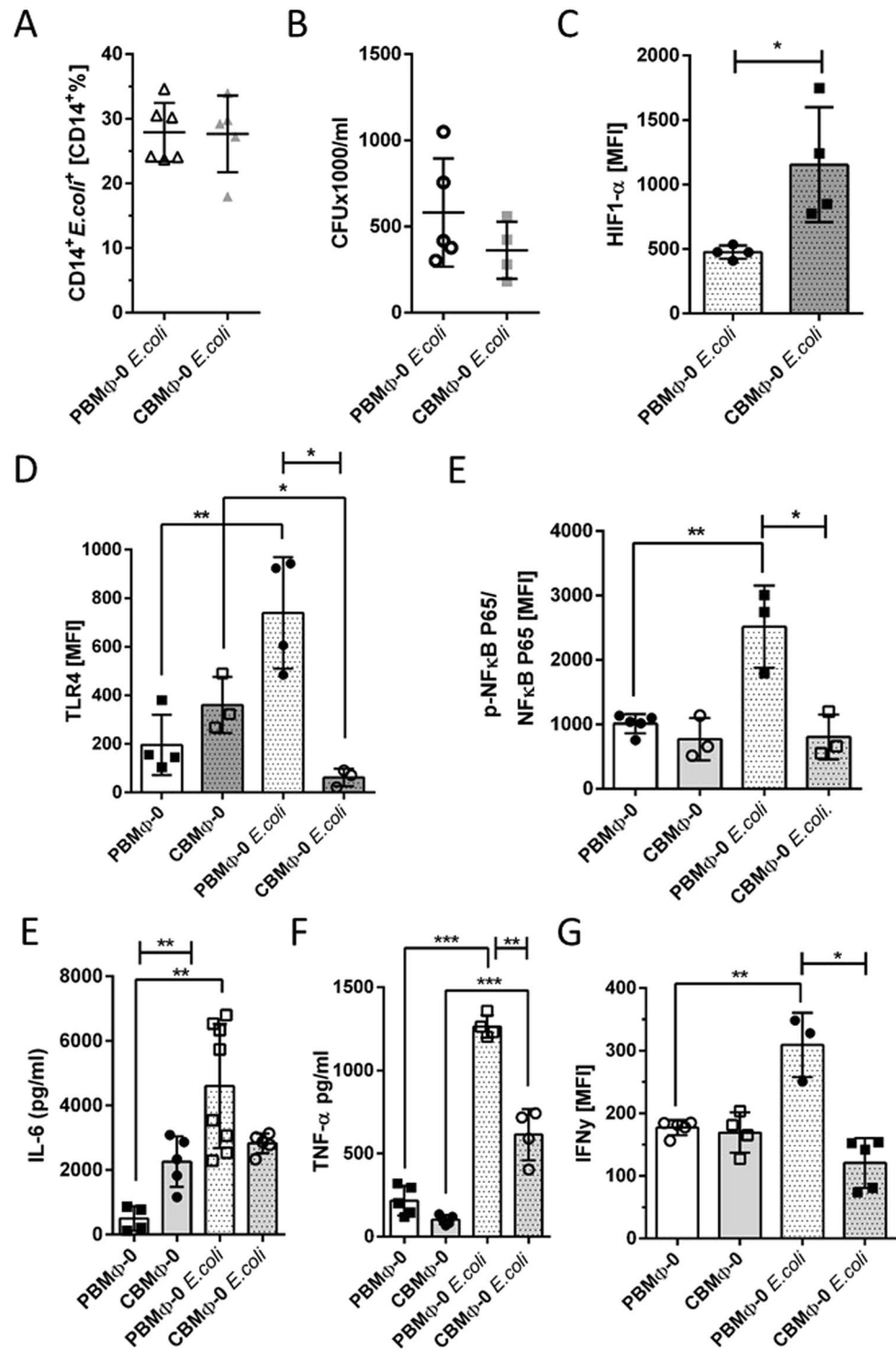


**Figure 2.** Periphagocytic reactions after infection with *E. coli*. Phagocytic indices of indicated M $\Phi$  were assessed 4 h p.i. (post infection; A). Killing of *E. coli* was assessed 12 h p.i. (B). HIF-1 $\alpha$  expression was measured 12 h p.i. (C). Expression of TLR-4 (D) and phosphorylated NF $\kappa$ B-P65 (E) were assessed by FACS 4 h p.i. Secretion of IL6 (F) and TNF $\alpha$  (G) were determined by ELISA 12 h p.i. Intracellular production of IFN $\gamma$  (H) was also assessed (G, all charts, \* $p < 0.05$ , \*\* $p < 0.01$ , \*\*\* $p < 0.005$ ; bars, student's t-test, blunt-ended bars, two-way-ANOVA).

**Phagocytosis, intracellular killing, and cytokine production of infected M $\Phi$ -0.** In order to simulate the impact of sepsis, we infected (non-cytokine driven) M $\Phi$ -0 with *E. coli* and analysed their anti-pathogenic capacity: Phagocytic indices (PI; Fig. 2A) and ROS production of PBM $\Phi$ -0 and CBM $\Phi$ -0 were similar ( $224.4 \pm 44.3$  in

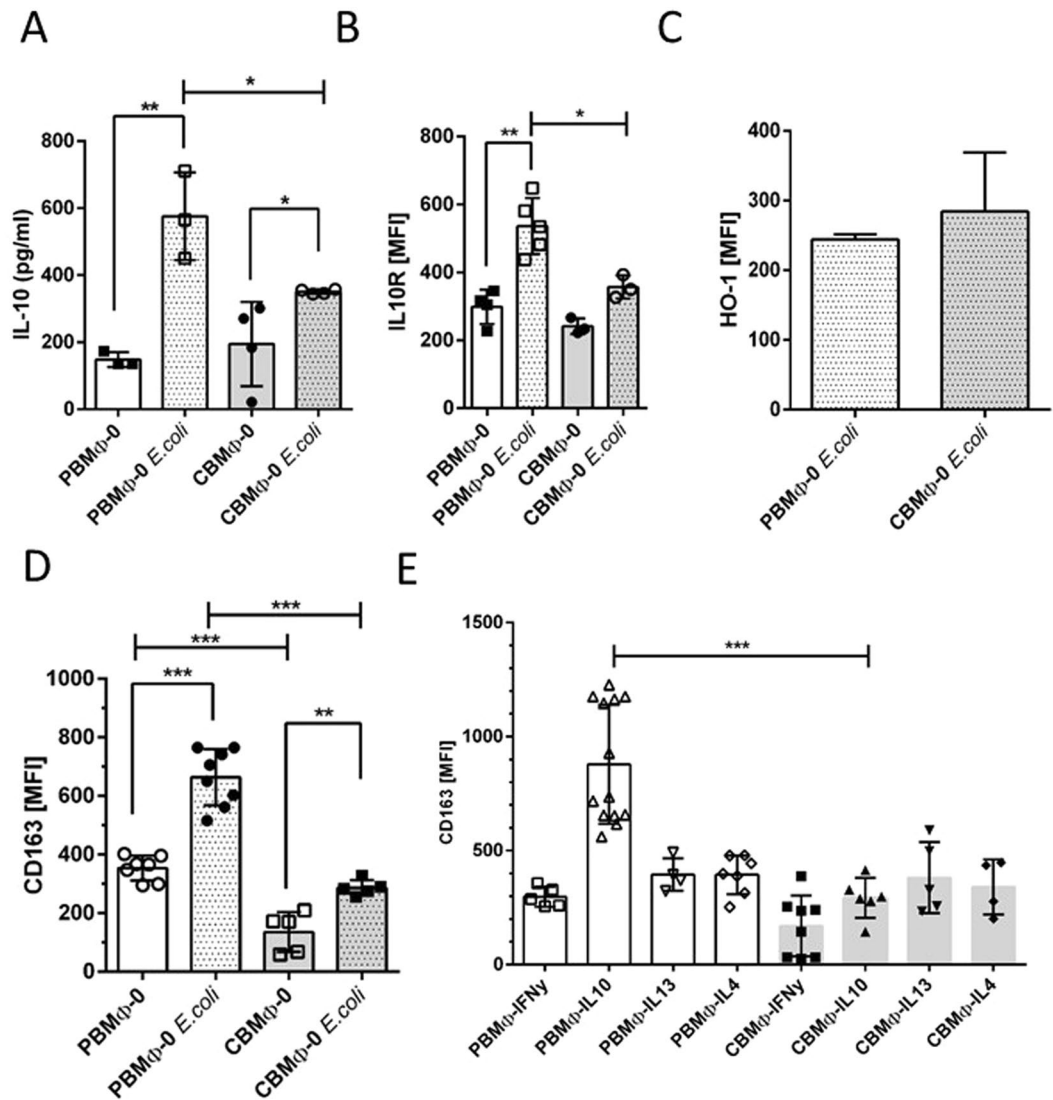


**Figure 3.** IL10 signaling and CD163 expression on MΦ-0 and MΦ-IL10. IL10 secretion was determined via ELISA (A). IL10R expression was assessed by FACS (B). Expression of HO-1 was measured 12 h p.i. (C). CD163 expression was quantified by FACS analysis of the indicated MΦ-0 groups (D,E), \* $p < 0.05$ , \*\* $p < 0.01$ , \*\*\* $p < 0.005$ ; forked bars, student's t-test, blunt bars, two-way-ANOVA).

PBMΦ-0 vs.  $221.7 \pm 70.4$  in CBMΦ-0). We as well detected no differences with regard to intracellular killing of bacteria (Fig. 2B). Starting from already higher HIF-1 $\alpha$  concentrations in the non-infected state (compare Fig. 1D first and 4<sup>th</sup> column), infected CBMΦ-0 up-regulated HIF-1 $\alpha$  twice as much as PBMΦ-0 (Fig. 2C). Despite this finding, infected PBMΦ-0 up-regulated TLR4 to significantly higher levels than CBMΦ-0, with a high phosphorylation of NF $\kappa$ B P65 (Fig. 2D,E). The latter is a transcription factor; its phosphorylation leads to a cascade of pro-inflammatory reactions in bacterially infected MΦ-0<sup>18</sup>. Likewise, the secretion of IL6, tumor-necrosis-factor-alpha (TNF $\alpha$ ), and IFN $\gamma$  was found higher in infected PBMΦ-0 (all  $p < 0.05$  vs. CBMΦ-0, Fig. 2E–G).

In non-infected PBMΦ-0 and CBMΦ-0, the secretion of IL10 was similar (Fig. 3A, first and third columns). After infection PBMΦ-0 and CBMΦ-0 both showed an increase in IL10 secretion, however, the increase was almost twice as high in PBMΦ-0 (Fig. 3A). For MΦ-IL10 polarisation, IL10 signaling is crucial<sup>19</sup>. The analysis of IL10-receptor (IL10R) expression after infection revealed that PBMΦ-0 up-regulated IL10R to a significantly higher level than CBMΦ-0 (Fig. 3B). Infection with *E. coli* did not enhance expression of HO-1, compared to the non-infected state (Fig. 1C).

IL10 is known to be a strong inducer of the scavenger receptor CD163<sup>20,21</sup>. Paralleled by the increase of IL10R and the IL10 secretion in infected PBMΦ-0 (Fig. 3A,B), we found a higher expression of CD163 in infected PBMΦ-0 (Fig. 3D), at a level comparable to non-infected PBMΦ-IL10. Polarisation with IL4 and IL13 did not lead to up-regulation of CD163 (Fig. 3E).

AKT phosphorylation occurred in PBMΦ-0 over twice as much as in CBMΦ-0 (Supplementary Fig. 3A), pointing to an engagement of mTOR. This activation pattern did not change in MΦ-IL10 (Supplementary



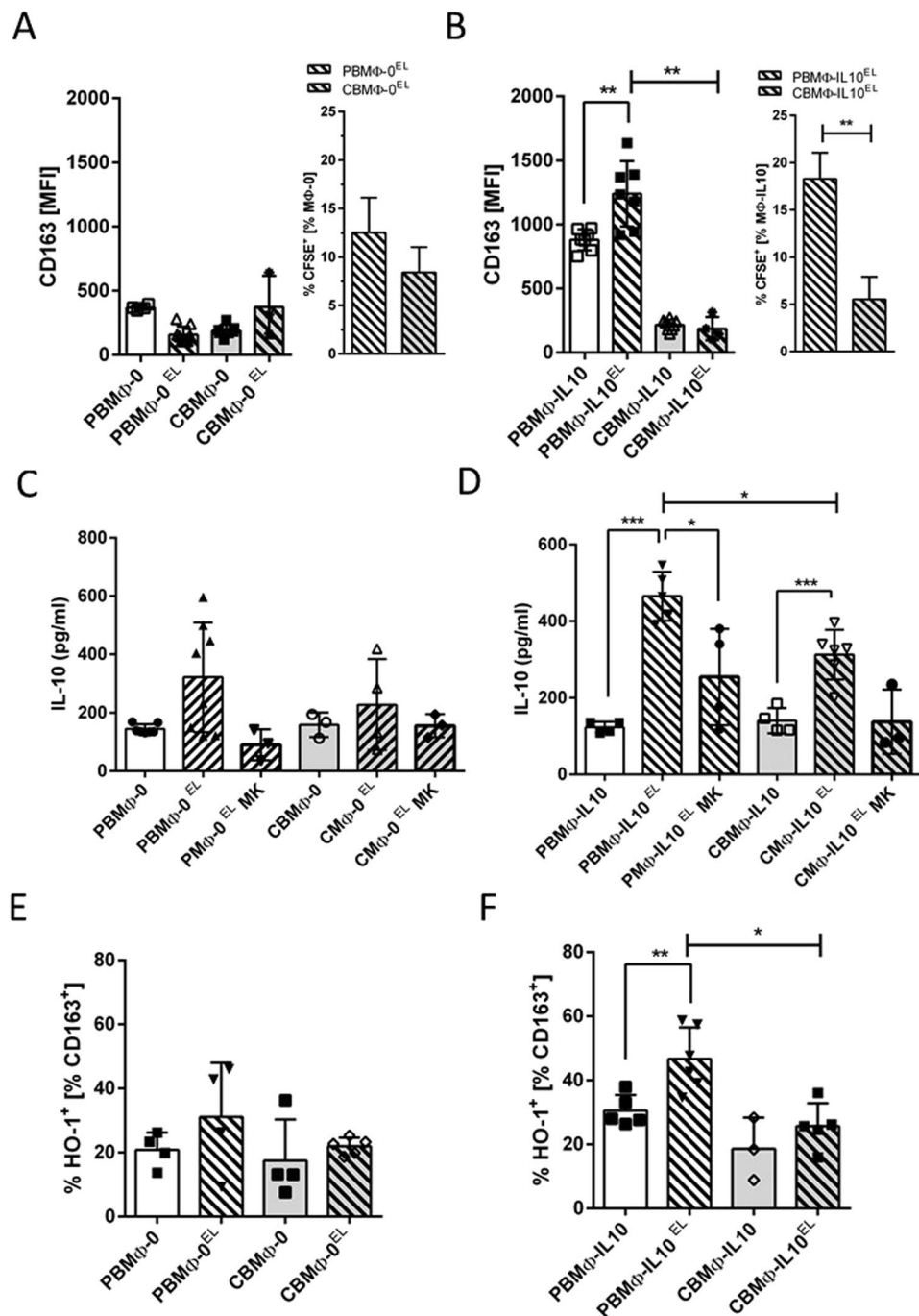


**Figure 4.** Regulation of CD163 expression, uptake of senescent erythrocytes (EL), IL-10 secretion, and assessment of HO-1 expressing MΦ. CD163 expression (A,B, left charts) and incorporation index (% of CFSE-positive MΦ) of senescent erythrocyte lysates (EL) were assessed 2h post treatment. (A,B, right charts). IL-10 secretion from MΦ-0 (C) and MΦ-IL10 (D) was measured 24 h post treatment (\* $p < 0.05$ , \*\* $p < 0.01$ , \*\*\* $p < 0.005$ , forked bars, student's t-test, blunt bars, two-way-ANOVA).

Fig. 3B). We had shown before<sup>11</sup> that mTOR signaling is reduced in CBMΦ. Rapamycin, an inhibitor of mTOR, did not reduce IL10 secretion of infected PBMΦ-0 but resulted in significantly lower expression of CD163 (Supplementary Fig. 2A,B). Taken together, these findings provide evidence that *E. coli* infection initiates comparable bactericidal reactions in PBMΦ-0 and CBMΦ-0 but differs in the PAMP dependent signaling, resulting in enhanced cytokine production.

**CBMΦ-IL10 show impaired clearing of senescent erythrocyte remnants.** We tested, whether the observed difference of CD163 expression on MΦ-0 and MΦ-IL10 (Fig. 3) would have functional consequences (Fig. 4). CD163 is involved in the clearance of Hb:Hp complexes, serum levels of which are elevated after birth,

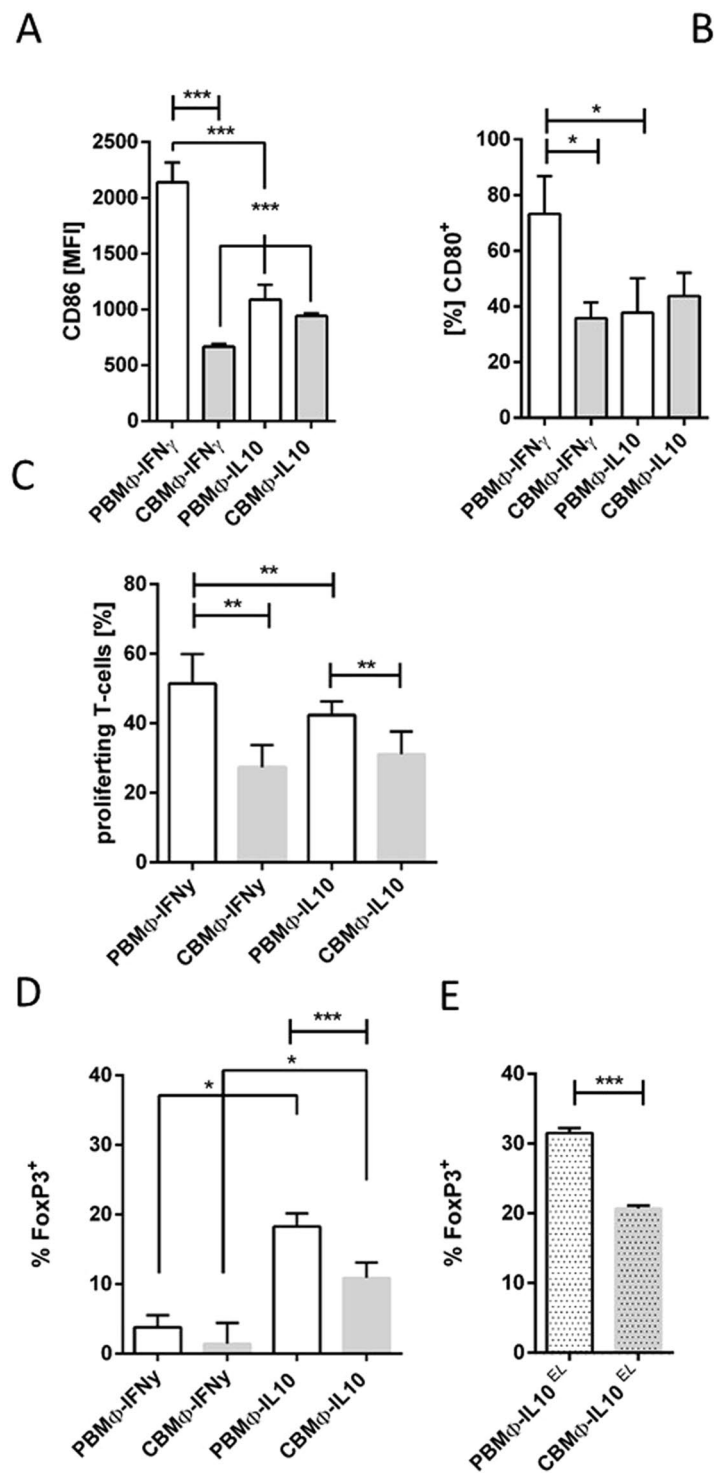


**Figure 5.** Polarisation of CBM $\Phi$  leads to alterations of B7 molecule expression, reduced T-cell blast formation and decrease of FoxP3 expressing T-cells. Expression of the B7-family molecules were assessed by flow cytometry for the indicated M $\Phi$  populations (A,C). Proliferation of non-infected T cells was measured by determination of T-cell blasts (B; decrease of mean CFSE fluorescence intensity as depicted in Supplementary Fig. 1D). Regulatory T-cells were characterized by intracellular FoxP3 staining within the population of CD4 positive lymphocytes (D). FoxP3 expressing T-cells were also quantified after addition of senescent erythrocytes (E; all charts n = 3; \*p < 0.05, \*\*p < 0.01, \*\*\*p < 0.005, student's t-test, simple bar, forked bars, two-way-ANOVA).

infection, trauma, and organ damage<sup>22,23</sup>. Therefore, we tested the capacity of M $\Phi$ s to take up senescent erythrocytes (EL). We co-cultured M $\Phi$ -0 (Fig. 4A,C,E) and M $\Phi$ -IL10 (Fig. 4B,D,F) with carboxyfluoresceinsuccinimidylester- (CFSE-) marked senescent erythrocytes as a source for Hb:Hp complexes and analysed the uptake.

Expression of CD163 on PBM $\Phi$ -0 and CBM $\Phi$ -0 was not altered after co-cultivation with EL (Fig. 4A left). In contrast, CD163 was up-regulated only in the PBM $\Phi$ -IL10 subtype (Fig. 4B left). Whereas the erythrocyte uptake of M $\Phi$ -0 was not different (Fig. 4A right), CBM $\Phi$ -IL10 incorporated fewer erythrocytes than PBM $\Phi$ -IL10 (Fig. 4B right). CD163 plasma-membrane expression was elevated on PBM $\Phi$ -IL10 co-cultured with EL compared to PBM $\Phi$ -0. This process could not be observed in CBM $\Phi$ . These data suggest a functional correlation between lower CD163 expression on CBM $\Phi$ , lower IL10 secretion, and their reduced clearance of erythrocytes.

**CD163 expression correlates to IL10-secretion and HO-1 expression in PBM $\Phi$ -IL10 after phagocytosis of erythrocytes.** Engagement of CD163 initiates PI3k/AKT signaling, which, again, leads to IL10 secretion by the cell<sup>24–26</sup>. PBM $\Phi$ -0 and CBM $\Phi$ -0 showed no significant differences in IL-10 secretion after co-cultivation with EL (Fig. 4C). For M $\Phi$ -IL10 a significant increase of IL-10 production was assessed 24 h p.i., but the concentration was significantly higher in PBM $\Phi$ -IL10 compared to CBM $\Phi$ -IL10 (Fig. 4D). Addition of the AKT inhibitor MK-2066 (MK) to EL treatment reduced IL-10 secretion in PBM $\Phi$ -IL10, suggesting that AKT signaling is engaged in this process. This finding was supported by phosphorylation of AKT in PBM $\Phi$ -IL10 and CBM $\Phi$ -IL10 (Supplementary Fig. 3D).

M $\Phi$  expressing HO-1 were not elevated in EL treated M $\Phi$ -0 (Fig. 4E). In contrast, more PBM $\Phi$ -IL10 expressed HO-1 compared to CBM $\Phi$ -IL10 (Fig. 4F). Taken together, the results suggest that an enhanced CD163 expression in PBM $\Phi$ -IL10 after EL exposure is attributed to increased IL-10 secretion and in turn HO-1 expression is up-regulated.

**T-cell stimulation and induction of FoxP3-positive regulatory T-cells under polarisation.** T-cell proliferation requires a variety of co-stimulatory molecules, e.g. CD80 and CD86, members of the B7-family. We assayed the surface expression of CD86 on polarised M $\Phi$  and found a significant reduction on CBM $\Phi$ -IFN $\gamma$  and CBM $\Phi$ -IL10 (Fig. 5A) compared to corresponding PBM $\Phi$ . In line with this finding we detected more CD80 expressing PBM $\Phi$ -IFN $\gamma$  (Fig. 5B). Since these receptors influence antigen presenting cell-dependent T-cell stimulation, we co-cultured polarised M $\Phi$  with T-cells and stimulated with  $\alpha$ CD3 mAb for 72 hours, as shown before<sup>27</sup>. We found adult T-cell blast formation profoundly reduced, when CBM $\Phi$ -IFN $\gamma$  and CBM $\Phi$ -IL10 were co-incubated as a source of co-stimulatory signals. Cord blood T-cell proliferation was diminished, as already known. (Fig. 5C).

Among other signals, IL10 is crucial for the expansion of regulatory T cells (Tregs<sup>28</sup>). We analysed the induction of FoxP3 among CD4<sup>+</sup> T cells (Fig. 5D). Whereas M $\Phi$ -IFN $\gamma$  subtypes induced equivalent proportions of FoxP3 expressing T cells, their induction under IL10 polarisation was significantly augmented by PBM $\Phi$  ( $p < 0.05$  vs. CBM $\Phi$ ). EL treatment enhanced the expansion of FoxP3<sup>+</sup> Tregs in both PBM $\Phi$ -IL10 and CBM $\Phi$ -IL10 (Fig. 5E). Taken together, the reduced expression of B7 molecules on polarised CBM $\Phi$  compared to PBM $\Phi$  may be attributed to lower T cell expansion and a reduced Treg population in CBM $\Phi$ .

## Discussion

Like circulating monocytes, M $\Phi$  play a central role in shaping the immune response by production of bactericidal molecules, cytokines and by their phagocytic activity. Since neonatal sepsis is often followed by inflammatory organ damage, and since local tissue M $\Phi$  are extremely difficult to obtain, we decided to polarise monocyte-derived macrophages by preconditioning with M-CSF and additional treatment with either IFN $\gamma$ , or IL10. These microenvironments mirror the acute inflammatory phase as well as the resolving phase of infection and may help to decipher the functional differences of neonatal M $\Phi$  *in-vivo*.

In our previous publication, CBM $\Phi$  (M $\Phi$ -IFN $\gamma$ , M $\Phi$ -IL10) were characterized by a reduced capability to express M $\Phi$ -IL10 driven receptor signaling cascades<sup>11</sup>. Our present data suggest that neonatal CBM $\Phi$ -0 polarise aberrantly due to a crucial role for deficient intracellular signal transduction via STAT1, STAT3, NF $\kappa$ B, and HO-1 (Figs. 1, 2): In PBM $\Phi$ -0, the pSTAT3/pSTAT1 balance outweighs pSTAT1 and concomitantly shifts polarisation towards a non-inflammatory status. This balance is compromised in CBM $\Phi$ -0, which may be attributed to a lower susceptibility to the M-CSF signal, due to a tolerance generated by elevated M-CSF levels during pregnancy<sup>29,30</sup>, although M-CSF concentrations of the current *in-vitro* polarisation protocol were chosen to be high enough to level out these differences.

HO-1, which classifies as an anti-inflammatory factor<sup>31</sup>, was equally expressed in PBM $\Phi$ -0 and CBM $\Phi$ -0 (Fig. 1D). HIF-1 $\alpha$  is regarded as a pro-inflammatory key molecule<sup>32</sup>; its significantly stronger expression in CBM $\Phi$ -0 extenuated the anti-inflammatory bias of HO-1 expression (Fig. 1C). With the exception of IL6, the basal cytokine expression was similar in PBM $\Phi$ -0 and CBM $\Phi$ -0 (Fig. 2E–G).

IFN $\gamma$  skewed the pSTAT3/pSTAT1 balance in PBM $\Phi$ -IFN $\gamma$  but failed to do so in CBM $\Phi$ -IFN $\gamma$  (Fig. 1A,B, second vs. third columns), confirming earlier results<sup>33</sup>. CBM $\Phi$ -IFN $\gamma$  exhibited high HIF-1 $\alpha$  expression but an inadequate pSTAT1 activation (Fig. 1A,C). This can be caused by a crosstalk via IL6 and pSTAT3<sup>34</sup>. The aberrant pSTAT3 up-regulation in CBM $\Phi$ -IL10 resulted in a diminished HO-1 expression (Fig. 1D), concordant with previous results supporting the hypothesis for a diminished anti-inflammatory polarisation of CBM $\Phi$ <sup>11</sup>.

Addressing the question whether naïve CBM $\Phi$ -0 reacted on pathogen-associated-molecule-pattern (PAMP) comparable to PBM $\Phi$ -0, we found no significant differences in bacterial killing (Fig. 2A,B), but a diminished secretion of both, pro- (i.e. TNF $\alpha$  and IL6; Fig. 2E–G) and IL10 (Fig. 3B). Studies with LPS activated PBM $\Phi$ <sup>35</sup> show similar results as we have seen with *E. coli* infected PBM $\Phi$ -0. The reduced cytokine production in CBM $\Phi$ -0 is caused by a weaker NF $\kappa$ B and TLR4 response (Fig. 2D,E). A diminished IL10 sensitivity towards IL10 in CBM $\Phi$ <sup>12</sup>, and a reduced production in CBM $\Phi$  after LPS treatment, support our observation<sup>36</sup>. To our knowledge, we showed for the first time that the IL10R is down-regulated on the plasma-membrane of CBM $\Phi$ -IL10, suggesting that IL10-/IL10R-signaling is dampened (Fig. 3B,C).



Compared to the non-infected M $\Phi$ -0, *E. coli* challenged CBM $\Phi$ -0 upregulated HIF-1 $\alpha$  more strongly compared to PBM $\Phi$ -0 (Fig. 2C, compare to Fig. 1C, first and 4<sup>th</sup> columns). HO-1 was not up-regulated after *E. coli* infection (Fig. 3C, compare to Fig. 1D, first and 4<sup>th</sup> columns), although HIF-1 $\alpha$  up-regulates HO-1 expression to enable the transition from pro- to anti-inflammatory reactions<sup>37</sup>. To deploy its function, HIF-1 $\alpha$  requires IL10<sup>38</sup>, which we found reduced in *E. coli* challenged CBM $\Phi$ -0.

*E. coli* infection is attributed to IL10 secretion and CD163 up-regulation in PBM $\Phi$ -0 and PBM $\Phi$ -IL10 (Fig. 3A,D). CD163 was not up-regulated in M $\Phi$ -IL4 and M $\Phi$ -IL13 (Fig. 3E). In contrast, addition of IL-10 to CBM $\Phi$  had no effect on CD163 expression, most likely due to a scarcity of the IL10R (see above, Fig. 3D).

The sequestration of iron and derivatives is a crucial function of M $\Phi$ , depending from the transient polarisation status, since iron is an energy source for pathogens<sup>38</sup>. Iron containing hemoglobin is a product of inflammation, causes hemolysis and is bound by haptoglobin<sup>39</sup>. The Hb:Hp complexes in turn are bound and internalized by CD163<sup>40</sup>. We, therefore, compared the capacity of M $\Phi$ -0 as well as M $\Phi$ -IL10 (Fig. 4).

The detection of comparable erythrocyte uptake rates in PBM $\Phi$ -0 and CBM $\Phi$ -0 (Fig. 4A) can be explained by CD163 independent phagocytosis mediated by Fc- $\gamma$  receptors. The expression of CD163 and functional erythrocyte uptake could be seen for PBM $\Phi$ -IL10 and CBM $\Phi$ -IL10 (Fig. 4B). Comparing the IL-10 secretion and HO-1 upregulation of M $\Phi$ -0 and M $\Phi$ -IL10 upon EL challenge (Fig. 4C,F), we found more PBM $\Phi$ -IL10 than CBM $\Phi$ -IL10 to secrete IL10. Moreover, a higher percentage of PBM $\Phi$ -IL10 upregulated HO-1 after EL challenge, suggesting a CD163 driven signaling to anti-inflammatory polarisation in adults, which is diminished in newborns. CD163 dependent HO-1 regulation could be a target for therapeutic strategies, since HO-1 reduces oxidative stress, which is one of the main triggers for bronchopulmonary disease (BPD)<sup>41</sup>.

AKT dependency for IL10 secretion was also demonstrated by its pharmacological inhibition, utilizing MK2260. IL10 secretion was inhibited, but not entirely blocked (Fig. 4D, 4<sup>th</sup> and 6<sup>th</sup> column). The fact, that AKT signaling is not entirely linked to CD163 expression can be explained by the antagonistic function of the AKT isoforms AKT1 and AKT2 respectively<sup>42</sup>.

PBM $\Phi$ -IFN $\gamma$  but not CBM $\Phi$ -IFN $\gamma$  responded with increased presentation of B7-family molecules, resulting in an enhanced proliferation of T-cells (Fig. 5A–C). The reduced capacity of CBM $\Phi$ -IFN $\gamma$  to activate T-cells already has been demonstrated for CBM $\Phi$ <sup>27</sup>.

Regulatory T-cells (Tregs) control the immune response by suppressing pro-inflammatory reactions. We determined a higher percentage of FoxP3-positive T-cells in PBM $\Phi$ -IL10 polarised cultures (Fig. 5D). Our observation differs from findings in non-polarised conditions: In cord blood, suppressive Tregs were found increased compared to adult blood in the early phase after birth<sup>43</sup> and may expand under inflammatory conditions, e.g. necrotizing enterocolitis (NEC)<sup>44</sup>.

We interpret the results of the manuscript carefully: Since they are based on an *in-vitro* polarisation protocol, the concentrations of cytokines, the density of *E. coli* and erythrocyte lysates for the analysis of M $\Phi$  functions may only partially highlight differences. Since CD71<sup>+</sup> erythroid cells and MDSCs were reported to antagonize pro-inflammatory and bactericidal reactions, they could also contribute to the aberrant CBM $\Phi$  polarization, described here<sup>13,45</sup>. The *in-vitro* infection with *E. coli* neither exhibited a reduced phagocytosis nor resulted in an excessive survival of bacteria (Fig. 2A,B), suggesting that MDSC and erythroid cells did not downregulate this function and may not play a dominant role regarding to periphagocytic reactions. Future experiments are planned to elucidate this question.

Although a fast and effective systemic inflammatory response is a prerequisite against microbial invasion, it should resolve as soon as the microbes are eliminated. Delay or failure of inflammation-resolution processes leads to dysregulated and prolonged inflammation, which can damage organs and contribute to the development of malignant diseases, chronic lung disease, rheumatoid arthritis, type-2 diabetes mellitus, heart disease, and neurological disorders in adults<sup>46</sup>. It is known that sepsis-induced sustained inflammation may initiate and perpetuate brain damage of preterm infants via cytokine production and neuronal apoptosis<sup>10</sup>. The inflammatory response includes reactions that normally already contain components for its termination. This resolution is tightly regulated by effector cell apoptosis<sup>11,47</sup> and anti-inflammatory proteins, e.g. IL10 and transforming growth factor- $\beta$  (TGF- $\beta$ ). Not only do preterm infants appear to have a paucity of some of these anti-inflammatory factors<sup>48</sup>, but moreover their functional and metabolic response to IL10 is diminished<sup>11</sup>, leading to functional consequences<sup>12</sup> and a persistence of inflammatory cytokine production. Sustained neonatal systemic inflammatory response is associated with poor postnatal growth among infants born very preterm during the first year of life<sup>49</sup>.

The observations seen here, with a deficiency of cord blood monocytes to polarise into anti-inflammatory macrophage subtypes, together with a reduced induction of inhibitory Tregs, would blend into this model of sustained inflammation in neonatal sepsis and may offer new therapeutic targets.

## Materials and Methods

**Patients.** The study protocol was approved by the Ethics Committees of Aachen University Hospital (Permission No: EK150/09, Oct. 6, 2009, signed by Profs G. Schmalzing and U. Buell). All adult participants involved were informed and gave written consent to use their blood samples for this study participation. All term neonates were delivered spontaneously and did not exhibit signs of infection, as defined by clinical status, white blood cell count and C-reactive protein. Mothers with amnion infection and prolonged labour (>12 hours) were excluded. Umbilical cord blood was placed in heparin-coated tubes (4 IE/ml blood), immediately following cord ligation as described before<sup>50</sup>. All methods were performed in accordance with the relevant guidelines and regulations.

**Reagents.** Antibodies to CD4 (RPA-T4), CD80 (clone L307.4), CD86 (clone FUN 1), CD163 (clone GH1/61), HLA-DR (clone G46-2.6), TLR4 (clone HTA125), IL10 (clone JES3-9D7), FoxP3 (PCH101), TNF $\alpha$  (clone Mab11), HO-1 (clone MA1112), HIF-1 $\alpha$  (polyclonal goat IgG), CD71 (LO1.1) and Ig-matched controls (IgG1,

IgG2b) were from BD Biosciences (Heidelberg, Germany), eBiosciences (Frankfurt, Germany) and Immunotools (Friesoythe, Germany). Isopropyl- $\beta$ -D-thiogalactopyranoside (IPTG) and antibiotics were purchased from Sigma (Munich, Germany). Staining was performed according to the manufacturer's recommendations. Cytokines IFN $\gamma$ , IL4, IL10, M-CSF were from PAN Biotech (Aidenbach, Germany). CFSE was purchased from Molecular Probes (Eugene, OR, USA). RPMI was from Gibco (Paisley, UK). Green-fluorescent-protein (GFP) expressing *E. coli* were grown and used in infection assays as described before<sup>50</sup>. The phagocytosis index (CD14+ GFP+ M $\Phi$  %: CD14+ M $\Phi$  %) and the phagocytic capacity (mean fluorescent intensity (MFI) of CD14+ monocytes) were assessed by flow cytometry after 4 h p.i. (post infection) and 24 h p.i. For bacterial phagocytosis assays a multiplicity of infection of 25 (MOI25) was utilized. The AKT inhibitor MK 2206 was provided by Sellekchem and added 60 min before stimulation of cells at a final concentration of 1  $\mu$ M.

In our experiments, we could not observe significant differences in bacterial killing, which could be due to the fact that we used polarised macrophages and the studies cited before conducted experiments with monocytes. As a control for purification, we stained for CD71<sup>+</sup>: The M $\Phi$  populations generated *in-vitro* only contained few CD71<sup>+</sup> positive cells as revealed in FACS based staining. Unpurified mononuclear cells from cord blood contained about 50% erythroid cells (57.35%  $\pm$  24.34), whereas CBM $\Phi$ -IL10 only contained 8% erythroid cells (8.22%  $\pm$  1.9) on day 5.

**Differentiation protocols.** Our polarisation protocol followed the protocols published earlier<sup>1</sup>. In brief, leukocytes were prepared by density gradient centrifugation of whole blood from healthy adult donors and cord blood from term neonates as described before<sup>50</sup>. Polarisation was induced by seeding  $5 \times 10^5$  cells/ml in 12-well tissue culture cells and administration of 100 ng/ml MCSF for 72 h in RPMI (designated as M $\Phi$ -0). Where indicated further polarisation was achieved by addition of 50 ng/ml IFN $\gamma$  (designated as M $\Phi$ -IFN $\gamma$ ), 10 ng/ml IL4 (designated as M $\Phi$ -IL4) or 10 ng hIL10 (designated as M $\Phi$ -IL10) for additional 48 h. For T-cell polarisation assays the cell number was adjusted to  $5 \times 10^6$  cells/ml in 6-well culture plates.

T-cell proliferation assays were performed as published<sup>27</sup>. In brief, lymphocytes were isolated and split into two groups. One group was left untreated while the other group was subjected to the differentiation protocol as described<sup>11</sup>. Then, untreated, syngeneic lymphocytes were co-cultivated with the M $\Phi$  population as indicated in presence of stimulatory antibody OKT-3 for two additional days before analysis.

**Stimulation of M $\Phi$  with senescent erythrocyte lysates.** After Ficoll density separation, layers containing leucocytes, erythrocytes and serum were separated. The leukocyte suspension was subjected to the macrophage polarisation procedure described above. The erythrocyte fraction (80% hematocrit) was submitted to a second centrifugation step of  $10,000 \times g$  for 15 min. The lower 10% fraction was collected representing senescent erythrocytes<sup>51</sup>, which were resuspended in the autologous serum and further diluted 1:1 in phosphate buffered saline (PBS).

The senescent erythrocyte/serum suspension was stored at 4 C $^\circ$  for 5 days. Afterwards the erythrocyte/serum suspension was centrifuged ( $300 \times g$ , 15 min). The supernatant was stored for later usage. Pelleted erythrocytes were stained with CFSE according to standard protocols. After washing to remove excessive CFSE, labelled erythrocytes were resuspended in the supernatant collected before the CFSE staining procedure.

Polarised macrophages were detached from culture plates by adding PBS/EDTA (10 mM EDTA v/v, 10 min). The cell count of the CFSE-stained erythrocytes and the macrophage was measured using flow cytometry (FACS Canto II, see below), thereby controlling CFSE staining efficacy. M $\Phi$  and CFSE-stained erythrocytes were mixed in a ratio 1:100 and further cultivated under standard conditions (RPMI, 10% v/v FCS, 37 C $^\circ$ , 5% CO $_2$ ). It was previously reported that senescent erythrocyte suspensions release Hb and Hb:Hp complexes<sup>52</sup>. Phagocytosis and peri-phagocytic reactions were assessed as described in the result section. Co-cultivation of M $\Phi$  with senescent erythrocyte lysates were designated with the abbreviation EL.

Intracellular intermediates, cytokine and transcription factor detection.

For detection of reactive-oxygen-species (ROS), the ROS detection kit (eBiosciences, Frankfurt, Germany) was used according to the manufacturer's recommendations. Cells were fixed in 1% paraformaldehyde for 1 hour and permeabilized with 0.1% v/v Triton-X100 in PBS for 5 min. Afterwards cells were washed and blocked with PBS/FCS (5% v/v) for 20 min at room temperature (RT). Cells were washed again and stained with fluorochrome labelled antibodies in PBS/FCS (5% v/v) for 60 min at RT followed by additional washing. Intracellular staining of human peripheral blood mononuclear cells (PBMCs) with PCH101 antibody was done using the anti-human Foxp3 staining set from eBioscience following the manufacturer's recommendations.

**Flow cytometry.** A daily calibrated FACS-Canto flow cytometer (Becton Dickinson, MountainView, CA) was used to perform phenotypic analysis. To prevent nonspecific binding, cells were incubated with 10% fetal calf serum on ice for 10 minutes before staining with pacific-blue (PB)-, fluorescein-isothiocyanate (FITC)-, phycoerythrin (PE)-, allophycocyanin (APC)-, or anti-IgG secondary -labelled monoclonal antibodies for 20 minutes on ice in the dark. Monocytes were gated using forward scatter (FSC), side scatter (SSC), and CD14 expression. The gating strategy and typical analysis is provided in Supplemental Fig. 1.

**ELISA.** The TNF $\alpha$  and IL10 enzyme-linked immunosorbent assays (ELISA) were purchased from eBiosciences (Ebiosciences-Natutec, Frankfurt, Germany) and used according to the manufacturer's recommendations. The IL6 ELISA was purchased from Immunotools (Friesoythe, Germany). The read-out was executed in a spectra max 340PC ELISA reader (molecular devices, Sunnyvale, CA, USA) with a sensitivity from 4–500 pg/ml.

**Western blot.** For the immunoblot analysis,  $6 \times 10^6$  cells were subjected to SDS-PAGE which was performed according to standard protocols. For imaging and quantification, a LAS 3000 imager (Fujifilm, Düsseldorf, Germany) combined with the Multi-Gauge software (Fujifilm, Düsseldorf, Germany) was used.

**Statistical analysis.** Results are expressed as mean  $\pm$  standard deviation. Error bars represent standard deviations. Values of  $p < 0.05$  were considered significant. Analyses were done with statistical software performing student's t-test and two-way ANOVA. Experiments with  $N = 3$  were tested according to Mann-Whitney for significant difference. Data which did not pass a test for Gaussian distribution were tested with a Kolmogorov-Smirnov test as provided by Graph Prism Pad Software Statistical Package, La Jolla, CA 92037 USA.

### Data availability

The datasets generated during and/or analysed during the current study are not publicly available but are available from the corresponding author on request. The authors declare to make materials, data and associated protocols promptly available to readers after acceptance of the manuscript and will upload all original data to a repository.

Received: 19 September 2019; Accepted: 17 December 2019;

Published online: 17 January 2020

### References

1. Rey-Giraud, F., Hafner, M. & Ries, C. H. *In vitro* generation of monocyte-derived macrophages under serum-free conditions improves their tumor promoting functions. *PLoS One*. **7**, e42656, <https://doi.org/10.1371/journal.pone.0042656> (2012).
2. Maeda, H. *et al.* TGF-beta enhances macrophage ability to produce IL-10 in normal and tumor-bearing mice. *J. Immunol.* **155**, 4926–4932 (1995).
3. Mantovani, A., Sica, A. & Locati, M. New vistas on macrophage differentiation and activation. *Eur J Immunol.* **37**, 14–16 (2007).
4. Biswas, S. K. & Mantovani, A. Macrophage plasticity and interaction with lymphocyte subsets: cancer as a paradigm. *Nat Immunol.* **11**, 889–896 (2010).
5. Martinez, F. O. & Gordon, S. The M1 and M2 paradigm of macrophage activation: time for reassessment. *F1000Prime Rep.* **6**, 13, <https://doi.org/10.12703/P6-13> (2014).
6. Martinez, F. O., Sica, A. & Locati, M. Macrophage activation and polarization. *Front. Biosci.* **13**, 453–461 (2008).
7. Murray, P. J. *et al.* Macrophage activation and polarization: nomenclature and experimental guidelines. *Immunity*. **41**, 14–20 (2014).
8. Röszer, T. Understanding the Mysterious M2 Macrophage through Activation Markers and Effector Mechanisms. *Mediators Inflamm.* **2015**, 816460, <https://doi.org/10.1155/2015/816460> (2015).
9. Landis, R. C., Quimby, K. R. & Greenidge, A. R. M1/M2 Macrophages in Diabetic Nephropathy: Nrf2/HO-1 as Therapeutic Targets. *Curr Pharm Des.* **24**, 2241–2249 (2018).
10. Dammann, O. & Leviton, A. Intermittent or sustained systemic inflammation and the preterm brain. *Pediatr Res.* **75**, 376–380 (2014).
11. Dreschers, S. *et al.* Impaired cellular energy metabolism in cord blood macrophages contributes to abortive response toward inflammatory threats. *Nat Comm.* **10**, 1685, <https://doi.org/10.1038/s41467-019-09359-8> (2019).
12. Gille, C. *et al.* Diminished response to interleukin-10 and reduced antibody-dependent cellular cytotoxicity of cord blood monocyte-derived macrophages. *Pediatr Res.* **60**, 152–157 (2006).
13. Elahi, S. *et al.* Immunosuppressive CD71+ erythroid cells compromise neonatal host defence against infection. *Nature.* **504**, 158–162 (2013).
14. Leiber, A. *et al.* Neonatal myeloid derived suppressor cells show reduced apoptosis and immunosuppressive activity upon infection with Escherichia coli. *Eur J Immunol.* **47**, 1009–1021 (2017).
15. Tu, G. *et al.* Glucocorticoid attenuates acute lung injury through induction of type 2 macrophage. *J Transl Med.* **15**, s12967, <https://doi.org/10.1186/s12967-017-1284-7> (2017).
16. Jiang, Z. & Zhu, L. Update on the role of alternatively activated macrophages in asthma. *J Asthma Allergy.* **9**, 101–107 (2016).
17. Liu, F. & McCullough, L. D. Inflammatory responses in hypoxic ischemic encephalopathy. *Acta Pharmacol Sin.* **34**, 1121–1130 (2013).
18. Lin, L. R. *et al.* Akt, mTOR and NF- $\kappa$ B pathway activation in Treponema pallidum stimulates M1 macrophages. *Int Immunopharmacol.* **59**, 181–186 (2018).
19. Melton, D. W., McManus, L. M., Gelfond, J. A. & Shireman, P. K. Temporal phenotypic features distinguish polarized macrophages *in vitro*. *Autoimmunity* **48**, 161–176 (2015).
20. Quimby, K. R., Greenidge, A., Harris, A. & Landis, R. C. Phenotypic commitment of monocytes towards a protective hemoglobin scavenging phenotype (CD14(pos)CD163(high)HLA-DR(low)) following cardiopulmonary bypass. *Cytometry B Clin Cytom.* **78**, 357–360 (2010).
21. Philippidis, P. *et al.* Hemoglobin scavenger receptor CD163 mediates interleukin-10 release and heme oxygenase-1 synthesis: antiinflammatory monocyte-macrophage responses *in vitro*, in resolving skin blisters *in vivo*, and after cardiopulmonary bypass surgery. *Circ Res.* **94**, 119–126 (2004).
22. Rubio-Navarro, A. *et al.* Hemoglobin induces monocyte recruitment and CD163-macrophage polarization in abdominal aortic aneurysm. *Int J Cardiol.* **15**, 66–78 (2015).
23. Subramanian, K., Du, R., Tan, N. S., Ho, B. & Ding, J. L. CD163 and IgG codefend against cytotoxic hemoglobin via autocrine and paracrine mechanisms. *J Immunol.* **190**, 5267–5278 (2013).
24. Komori, H. *et al.*  $\alpha(1)$ -Acid glycoprotein up-regulates CD163 via TLR4/CD14 protein pathway: possible protection against hemolysis-induced oxidative stress. *J. Biol. Chem.* **287**, 30688–30700 (2012).
25. Lim, J. E., Chung, E. & Son, Y. 1A neuropeptide, Substance-P, directly induces tissue-repairing M2 like macrophages by activating the PI3K/Akt/mTOR pathway even in the presence of IFN $\gamma$ . *Sci Rep.* **7**, 9417, <https://doi.org/10.1038/s41598-017-09639-7> (2017).
26. Landis, R. C., Philippidis, P., Domin, J., Boyle, J. J. & Haskard, D. O. Haptoglobin Genotype-Dependent Anti-Inflammatory Signaling in CD163(+) Macrophages. *Int J Inflamm.* **2013**, 980327, <https://doi.org/10.1155/2013/980327> (2013).
27. Dietz, S. *et al.* Cord blood granulocytic myeloid-derived suppressor cells impair monocyte T cell stimulatory capacity and response to bacterial stimulation. *Pediatr Res.* **86**, 605–615 (2019).
28. Nascimento, D. C. *et al.* IL-33 contributes to sepsis-induced long-term immunosuppression by expanding the regulatory T cell population. *Nat Commun.* **4**, 14919, <https://doi.org/10.1038/ncomms14919> (2017).
29. Ikeno, K. *et al.* A. Increased macrophage-colony stimulating factor levels in neonates with perinatal complications. *Early Hum Dev.* **46**, 229–237 (1996).
30. Praloran, V., Coupey, L., Donnard, M., Berrada, L. & Naud, M. F. Elevation of serum M-CSF concentrations during pregnancy and ovarian hyperstimulation. *Br J Haematol.* **86**, 675–677 (1994).
31. Abraham, N. G. & Drummond, G. CD163-Mediated hemoglobin-heme uptake activates macrophage HO-1, providing an antiinflammatory function. *Circ Res.* **99**, 911–914 (2006).
32. Braverman, J., Sogi, K. M., Benjamin, D., Nomura, D. K. & Stanley, S. A. HIF-1 $\alpha$  Is an Essential Mediator of IFN- $\gamma$ -Dependent Immunity to Mycobacterium tuberculosis. *J Immunol.* **197**, 1287–1297 (2016).

33. Maródi, L., Goda, K., Palicz, A. & Szabó, G. Cytokine receptor signalling in neonatal macrophages: defective STAT-1 phosphorylation in response to stimulation with IFN-gamma. *Clin Exp Immunol.* **26**, 456–460 (2001).
34. El Kasmi *et al.* Adventitial fibroblasts induce a distinct proinflammatory/profibrotic macrophage phenotype in pulmonary hypertension. *J Immunol.* **193**, 597–609 (2014).
35. Valero, N. *et al.* Differential induction of cytokines by human neonatal, adult, and elderly monocyte/macrophages infected with dengue virus. *Viral Immunol.* **27**, 151–159 (2014).
36. Chelvarajan, R. L. *et al.* Defective macrophage function in neonates and its impact on unresponsiveness of neonates to polysaccharide antigens. *J Leukoc Biol.* **75**, 982–994 (2004).
37. Komatsu, D. E. & Hadjiargyrou, M. Activation of the transcription factor HIF-1 and its target genes, VEGF, HO-1, iNOS, during fracture repair. *Bone* **34**, 680–688 (2004).
38. Cairo, G., Recalcati, S., Mantovani, A. & Locati, M. Iron trafficking and metabolism in macrophages: contribution to the polarized phenotype. *Trends Immunol.* **32**, 241–247 (2011).
39. Kato, G. J. Haptoglobin halts hemoglobin's havoc. *J Clin Invest.* **119**, 2140–2142 (2009).
40. Schaer, C. A., Schoedon, G., Imhof, A., Kurrer, M. O. & Schaer, D. J. Constitutive endocytosis of CD163 mediates hemoglobin-heme uptake and determines the noninflammatory and protective transcriptional response of macrophages to hemoglobin. *Circ Res.* **99**, 943–950 (2006).
41. Amata, E. *et al.* Role of the Nrf2/HO-1 axis in bronchopulmonary dysplasia and hyperoxic lung injuries. *Clin Sci (Lond).* **131**, 1701–1712 (2017).
42. Vergadi, E., Ieronymaki, E., Lyroni, K., Vaporidi, K. & Tsatsanis, C. Akt Signaling Pathway in Macrophage Activation and M1/M2 Polarization. *J Immunol.* **198**, 1006–1014 (2017).
43. Hayakawa, S., Ohno, N., Okada, S. & Kobayashi, M. Significant augmentation of regulatory T cell numbers occurs during the early neonatal period. *Clin Exp Immunol.* **190**, 268–279 (2017).
44. Pang, Y., Du, X., Xu, X., Wang, M. & Li, Z. Monocyte activation and inflammation can exacerbate Treg/Th17 imbalance in infants with neonatal necrotizing enterocolitis. *Int Immunopharmacol.* **59**, 354–360 (2018).
45. Dunsmore, G. *et al.* Erythroid Suppressor Cells Compromise Neonatal Immune Response against Bordetella pertussis. *J Immunol.* **6**, 2081–2095 (1996).
46. Tabas, I. & Glass, C. K. Anti-inflammatory therapy in chronic disease: challenges and opportunities. *Science* **339**, 166–172 (2013).
47. Hotchkiss, R. S. & Nicholson, D. W. Apoptosis and caspases regulate death and inflammation in sepsis. *Nat Rev Immunol.* **11**, 813–822 (2006).
48. Blahnik, M. J., Ramanathan, R., Riley, C. R. & Minoo, P. Lipopolysaccharide-induced tumor necrosis factor-alpha and IL-10 production by lung macrophages from preterm and term neonates. *Pediatr Res.* **50**, 726–731 (2001).
49. Cuestas, E., Aguilera, B., Cerutti, M. & Rizzotti, A. Sustained Neonatal Inflammation Is Associated with Poor Growth in Infants Born Very Preterm during the First Year of Life. *J Pediatr.* **205**, 91–97 (2019).
50. Gille, C. *et al.* Phagocytosis and postphagocytic reaction of cord blood and adult blood monocyte after infection with green fluorescent protein-labeled Escherichia coli and group B Streptococci. *Cytometry B Clin Cytom.* **76**, 271–284 (2009).
51. Biondi, C. *et al.* Senescent erythrocytes: factors affecting the aging of red blood cells. *Immunol Invest.* **31**, 41–50 (2002).
52. Theurl, I. *et al.* On-demand erythrocyte disposal and iron recycling requires transient macrophages in the liver. *Nat Med.* **22**, 941–951 (2016).

## Acknowledgements

Thanks to the team of midwives under the direction of R. Fakhrabadi and the Department of Obstetrics and Gynaecology at the University Hospital of Aachen, in particular E. Stickeler and T. Goecke, for coordinating the cord blood sampling. We like to thank V. Cerovic from the department of microbiology for critical reading.

## Author contributions

Conceptualization: T.W.O., S.D. Methodology: K.O., S.D., N.H., T.W.O. Software, computational analysis: S.D., K.O., N.H. Validation: S.D., T.W.O. Formal analysis: S.D., T.W.O., N.H., K.O. Investigation: S.D., N.H., K.O. Resources: K.T., T.W.O. Data curation: S.D., K.T., K.O. Writing (original draft preparation): S.D., T.W.O. Writing (review and editing): T.W.O., S.D., K.O., K.T. Visualization: S.D. Supervision: S.D., T.W.O. Project administration: T.W.O.

## Competing interests

The authors declare no competing interests.

## Additional information

**Supplementary information** is available for this paper at <https://doi.org/10.1038/s41598-019-56928-4>.

**Correspondence** and requests for materials should be addressed to T.W.O.

**Reprints and permissions information** is available at [www.nature.com/reprints](http://www.nature.com/reprints).

**Publisher's note** Springer Nature remains neutral with regard to jurisdictional claims in published maps and institutional affiliations.



**Open Access** This article is licensed under a Creative Commons Attribution 4.0 International License, which permits use, sharing, adaptation, distribution and reproduction in any medium or format, as long as you give appropriate credit to the original author(s) and the source, provide a link to the Creative Commons license, and indicate if changes were made. The images or other third party material in this article are included in the article's Creative Commons license, unless indicated otherwise in a credit line to the material. If material is not included in the article's Creative Commons license and your intended use is not permitted by statutory regulation or exceeds the permitted use, you will need to obtain permission directly from the copyright holder. To view a copy of this license, visit <http://creativecommons.org/licenses/by/4.0/>.

© The Author(s) 2020